AIP | Applied Physics Letters

Towards monomaterial p-n junctions: Single-step fabrication of tin oxide films and their non-destructive characterisation by angle-dependent X-ray photoelectron spectroscopy

Maciej Krzywiecki, Adnan Sarfraz, and Andreas Erbe

Citation: Applied Physics Letters **107**, 231601 (2015); doi: 10.1063/1.4937003
View online: http://dx.doi.org/10.1063/1.4937003
View Table of Contents: http://scitation.aip.org/content/aip/journal/apl/107/23?ver=pdfcov
Published by the AIP Publishing

Towards monomaterial p-n junctions: Single-step fabrication of tin oxide films and their non-destructive characterisation by angle-dependent X-ray photoelectron spectroscopy

Maciej Krzywiecki,[1,2,a)] Adnan Sarfraz,[1] and Andreas Erbe[1]
[1]*Max-Planck-Institut für Eisenforschung GmbH, Max-Planck-Str. 1, 40237 Düsseldorf, Germany*
[2]*Institute of Physics–CSE, Silesian University of Technology, Konarskiego 22B, 44-100 Gliwice, Poland*

(Received 27 June 2015; accepted 22 November 2015; published online 7 December 2015)

The application of a non-destructive method for characterization of electronic structure of an ultrathin $SnO_{1<x<2}$ layer synthesized by spin coating on Si wafers was demonstrated. Utilizing angle dependent XPS, we quantified stoichiometry changes inside the $SnO_{1<x<2}$ layers of thickness comparable with the electron attenuation length. The O/Sn concentration varied from 1.25 near the SnO_x surface to 1.10 near the substrate/overlayer interface. Deviations from ideal stoichiometry are caused by defects, and defect levels affect the band structure of the SnO_x layers. By investigation of the valence band region, followed by main core level position tracking, changes of electronic parameters like energy levels shift were identified. The results indicated a downward energy levels shift by 0.45 eV in SnO_x layers at the SiO_2/SnO_x interface. In combination with the detected upward energy levels shift in the substrate's electronic structure, these results suggest a negative charge displacement across the SiO_2 layer. As a consequence, there is a significant carrier concentration gradient in the layer, from a nearly insulating oxide at the SnO_x surface to a semiconducting one at the bottom of the SnO_x film. The results showed that the application of a simple and cost-effective method allows tuning the materials' properties towards the one-step fabrication of materials with ambipolar doping. © *2015 AIP Publishing LLC*. [http://dx.doi.org/10.1063/1.4937003]

Stoichiometric SnO_2 is an n-type semiconductor that finds use in, e.g., optoelectronics, gas sensing, and photovoltaics.[1,2] The intrinsic band gap for SnO_2 is 3.6 eV,[3] which makes the material almost insulating. The conductivity of the transparent tin oxide is then caused by the deviation from stoichiometry.[3] SnO, on the other hand, is characterized by ambipolar doping.[4,5] By combination of the two tin oxides, one has the unique possibility to obtain p-n junctions in the same material base,[6] still conserving the main advantage of tin dioxide: transparency in the visible range. Simultaneously, high carrier concentration gradients become necessary as the dimensions in modern devices drop below 10s of nanometers.[7] This letter describes the fabrication of a thin film p-n-junction on tin oxide basis and the detailed characterization of its electronic structure and chemical composition.

The surface properties have a crucial effect in technological applications. The surface is strongly dependent on the subsurface region, which in turn is vulnerable to influences from the substrate/layer interface—especially in the case of ultra-thin layers where the Debye screening length is of the order of the layer thickness. Although SnO and SnO_2 layers have been investigated,[8–10] a simultaneous, nondestructive analysis of the oxide layer structure and the substrate/oxide interface is missing. Typical methods for direct determination of depth-dependent composition and electronic properties are X-ray photoelectron spectroscopy (XPS) and Auger electron spectroscopy, combined with ion etching. Ion etching, however, destroys the sample surface and may cause alterations in the internal structure. Therefore, in this letter, we employ angle-dependent XPS (ADXPS) as a nondestructive method for characterization of chemical composition and electronic structure of ultrathin layers.

Numerous film preparation techniques have been employed for tin oxide films such as epitaxial growth,[11] laser-induced chemical vapor deposition,[12] rheotaxial growth and thermal oxidation,[13] rheotaxial growth and vacuum oxidation,[14] and atomic layer deposition.[15] These methods resulted in oxide layers with properties tuned to a desired application. However, their disadvantage is the requirement of advanced and expensive setups. The alternative is sol-gel synthesis connected with spin-coat deposition, which offers the possibility of good control of the deposition parameters and low production costs. This method is also suitable for the fabrication of materials with a significant carrier concentration gradient.[16]

Substrates from Si(100) wafers (SiMat) (n-type, P-doped, 5–10 Ω·cm) were cleaned in an ultrasonic bath by sequentially soaking them in acetone, isopropanol, and deionized water for 15 min per cycle. Then, the wafers were blown with nitrogen and dried in a furnace at 110 °C for 30 min. Tin oxide sol (0.025M) was prepared by mixing tin (IV) isopropoxide (VWR) with triethylamine (TEA; VWR) in a molar ratio of 1:2, and subsequent dilution with isopropanol (VWR). Substrates were first rinsed with 0.007M TEA in isopropanol and immediately dried with nitrogen. Spin-coat deposition (Spin-coater P6700, Specialty Coating Systems, Inc.) was conducted at 500 rpm for 2 s, 2000 rpm for 8 s, and 6000 rpm for 20 s. After deposition, the samples were dried in air for 10 min at 110 °C. Finally, samples were

a)Author to whom correspondence should be addressed. Electronic mail: Maciej.Krzywiecki@polsl.pl. Tel.:+48 (32) 237 20 01. Fax: +48 (32) 237 22 16.

annealed in a tube furnace at 550 °C for 4 h in ambient atmosphere.

ADXPS was carried out on a Physical Electronics PHI Quantera II spectrometer equipped with an Al-K_α (1486.74 eV) micro-focused source and a dual-beam charge neutralizer. The pass energy was set to 140 eV for the survey spectra (energy step of 0.4 eV and analyzer acceptance angle of ±4°) and 26 eV for individual core level spectra (energy step of 0.025 eV). The XPS system base pressure was 2×10^{-8} Pa. All XPS spectra were recorded with varying take-off angle (TOA, defined as an angle between analyzer axis and normal to the sample plane) from 0° to 70°.

XPS data were analyzed by curve fitting using the CASA XPS software.[17] Each peak was represented by a sum of Gaussian (70%) and Lorentzian (30%) lines. The secondary electron background was subtracted utilizing the Shirley function. The full width at half maximum (FWHM) of the same components was allowed to vary within a narrow range. We used the lowest possible number of components to obtain acceptably low residual values. The estimated uncertainty for a particular component energy position was 0.04 eV. Quantitative analysis, including component ratio determination, was done with the use of CASA XPS embedded relative sensitivity factors (RSFs) and algorithms. The binding energy (B.E.) scale was calibrated to Au $4f_{7/2}$ (84.0 eV).[18] The SiO_2 layer thickness was determined to be 2.0(2) nm by standard ADXPS procedures.[19]

The estimation of information depth was based on the algorithm introduced by Opila and Eng, Jr.,[20] which is also utilized by major equipment manufacturers.[21] The algorithm is based on the assumption that the intensity I of the photoelectron signal, as a function of information depth, d, can be approximated as:[20] $I = I_0 e^{-d/\lambda \cos\theta}$, where I_0 is the intensity at the bare surface, λ is the electron escape depth, and θ is the TOA. The total thickness of the SnO_x layer was determined as 3.8(2) nm basing on a procedure proposed by Cumpson following the equation:[22]

$$\ln\left(\frac{\frac{I_f}{s_f}}{\frac{I_s}{s_s}}\right) - \left(\frac{\lambda_f}{\lambda_s} - \frac{1}{2}\right)\frac{t}{\lambda_0 \cos\theta} - \ln 2 = \ln\sinh\left(\frac{t}{2\lambda_f \cos\theta}\right), \quad (1)$$

where t is the film thickness, I_f and I_s are the measured peak intensities from film and substrate, respectively, s_f and s_s are their sensitivity factors, and λ_f and λ_s are the attenuation lengths of photoelectrons within the overlayer that originated in the overlayer and the substrate, respectively

The inelastic mean free path (IMFP) was estimated basing on analysis proposed by Werner,[23] using the TPP-2M (Tanuma-Powell-Penn[24]) algorithm embedded in NIST electron inelastic mean free path database.[25] The estimated depth uncertainties are mainly arising from the uncertainty of IMFP calculations involved in the TPP-2M predictive formula and were calculated by the uncertainty propagation method.[26] The uncertainties are a combination of two factors: (i) systematic errors which take into account possible charging effects[27,28] and (ii) random errors which can occur during the experiment. The significantly bigger uncertainty for the bigger information depths is attributed to so-called angular broadening.[29] In the present study, the information depth of 0 nm corresponds to the study of the SiO_2/SnO_x interface.

The depth estimation involved the following assumptions: (i) about 65% of the signal in electron spectroscopy will emanate from a depth of less than electron attenuation length λ_a (with this assumption $\lambda_a = \lambda$),[30] (ii) photoelectron diffraction and scattering are negligible, (iii) the layer is continuous, (iv) the X-ray intensity is essentially unattenuated throughout the analyzed volume, and (v) the λ_a is constant within the examined layer.

The inset of Figure 1 presents the O 1s and Sn 3d B.E. regions for TOA = 45°. The spin-orbit splitting is clearly visible for the Sn 3d region. The two distinct components in the O 1s region can be attributed to tin-bound oxygen (lower B.E.) and silicon oxide (higher B.E.) from the substrate.[31] Figure 1 presents the O/Sn ratio as a function of the information depth. The presented O/Sn ratio does not include the oxygen bound in interfacial SiO_2. The O/Sn ratio is varying from 1.10 to 1.25. Hence, the variation in IMFP based on TPP-2M calculations can be neglected, as it is ≈3%.

The decrease of the O/Sn concentration for information depth >3.5 nm can be attributed (i) to organic residues within the first nm and (ii) to increasing deviations caused by the more "grazing angle" of the measurement.

Since it is ambiguous to directly determine the tin oxidation state only on the basis of the Sn 3d region (Sn^{II} and Sn^{IV} binding energies are separated by less than 0.4 eV, Refs. 31–33), auxiliary tin oxidation state analysis was performed by investigation of the Auger MNN transition.[34] The Sn MNN region is presented as an inset in Figure 2(a). The chemical state of examined species is determined from the energy difference between a representative XPS peak and a suitable Auger peak. The Auger parameter α is defined as[34,35]

$$\alpha = E_k(MNN) + E_B(3d), \quad (2)$$

where $E_K(MNN)$ is the kinetic energy of the Auger transition MNN and E_B(3d) is the binding energy of an electron in

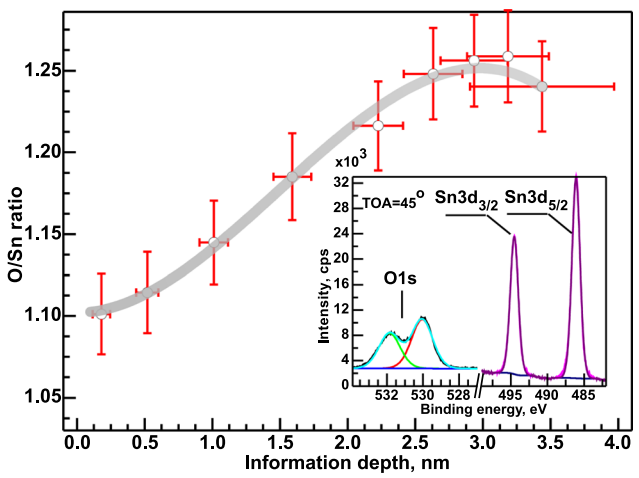

FIG. 1. O/Sn concentration ratio as function of information depth. The inset presents the O 1s and Sn 3d regions for TOA = 45°.

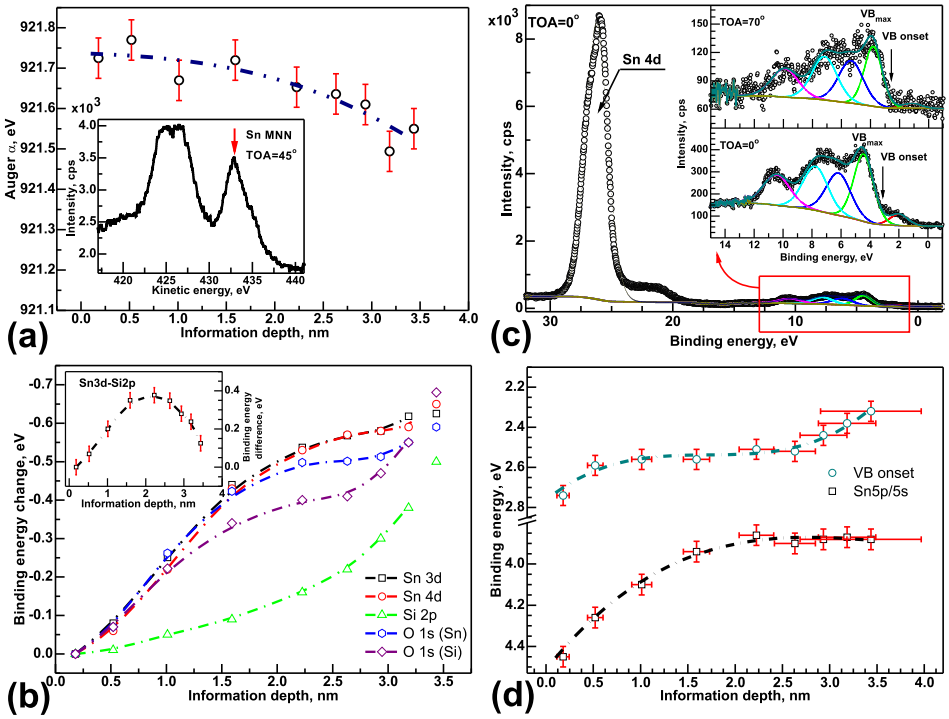

FIG. 2. (a) Auger α-parameter; inset: example of Auger Sn MNN at TOA = 45° with marked component employed for α-parameter analysis; (b) core level shift of Sn 3d, 4d, Si 2p (non-oxidized silicon), and O 1s (independently for O-Sn and O-Si contributions) core lines; inset: Sn 3d-Si 2p core level difference; (c) example of VB and Sn 4d region; insets: magnification of VB region for two TOAs; (d) binding energy for VB onset (VB_{onset}) and VB maximum (VB_{MAX}) as a function of estimated information depth. All curves in panels (a), (b), and (c) were fitted with polynomials.

atomic level Sn $3d_{5/2}$. A lower α indicates a lower electron density at the Sn atom, i.e., a higher oxidation state.[34]

Figure 2(a) shows α as a function of information depth. A change of the Sn oxidation state is clearly visible from the plot. This change is small, but supports the change in oxidation state obtained from analysis of the O/Sn ratio from XPS data (see Figure 1). The oxidation of Sn is lower in the vicinity of the substrate and higher at the layer's surface. Peak shape and position of the Sn MNN peak proved that the obtained material is in between SnO and SnO_2, but closer to SnO.[36,37] Furthermore, co-existence of different Sn oxidation states is possible.[34,38–40]

The detailed analysis of the Sn 3d/4d, Si 2p (substrate, non-oxidized silicon), and O 1s (independently for O-Sn and O-Si components) core level chemical shifts [Figure 2(b)] shows a clear shift of the Sn core levels toward higher binding energies with decreasing depth. A similar situation is observed for the substrate's Si 2p level; however, the slope is different: when the Sn 3d changes rapidly, the Si 2p changes are moderate. When probing the outmost part of the overlayer, the recorded substrate signal originates from the Si/SiO_2 interface. Consequently, when the vicinity of SiO_2/SnO_x is being probed, the majority of Si related signal originates from bulk substrate. The direction of the changes suggests downward energy levels shift in the SnO_x layer and an upward energy levels shift in the Si substrate at the Si/SiO_2 interface. However, the variation of binding energies comprises the chemical shift and the changes in local electrostatic potential.[41–43] At a given depth, the binding energy measured for core lines consists of potential shift of the same magnitude. Hence, the direct comparison of O 1s, Sn 3d/4d, and Si 2p core lines shows that the contribution of the chemical shift is at the level of ∼0.20 eV. The analysis leads also to conclusion that the maximal (global) impact of the electrostatic potential across the SnO_x overlayer is at maximum ∼0.4 eV. For the substrate, this contribution is significantly lower as shown by a comparison of the O1s (Si) line with Si 2p core line.

Moreover, the energy distance between Sn and Si core levels [inset in Figure 2(b)] shows that a chemical interaction, i.e., a charge transfer, over the substrate/overlayer interface is highly probable.[44]

More details emerge from the analysis of the valence band (VB) region. Figure 2(c) presents the VB region together with the Sn 4d core level for TOA = 0°. The insets of Figure 2(c) present the magnification of the VB region for the highest and lowest TOA. The shift of the VB onset is well visible. The VB onset was determined by the approximation of the slope of the valence band (VB_{MAX}) peak. The VB is the level originating from mixing of the O 2p and Sn 5s orbitals.[45,46] The changes of VB onset (E_V) and VB_{MAX} positions as a function of the information depth (Figure 2(d)) show that the shapes of the changes are not identical. While the VB_{MAX} shift follows the shift in the Sn3d/4d positions, E_V remains almost constant between 0.5 and 2.5 nm of information depth. This deviation has its origin in the presence of an additional component at the low binding energy side of the VB_{MAX} (small red component in inset of Figure 2(d) for TOA = 0°). This component is strongly affecting the spectrum of the VB region, impacting both the position and the shape of the VB components. The fact that the component is well detectable only for TOA < 40° suggests that it is substrate-related. The determined energy difference to the component's onset to the Fermi level (B.E. = 0) of 0.62 eV suggests also a substrate origin. The broad peak shape causing the increase of the background in this region suggests that this component is not originating from a simple bulk component, however. The most probable cause for this feature are defect sites related to oxygen vacancies (V_O) in the vicinity of the substrate/overlayer interface. The shape of the VB_{onset} - VB_{MAX} distance (and consequently E_F–E_V) changes indicates that several factors of competing nature—

some increasing, others decreasing the overall density of states—are present near E_V. While V_O will act as deep donors,[46] Sn vacancy (V_{Sn}) in the subsurface region of the SnO_x layer will act as a shallow acceptor.[47,48] V_O and V_{Sn} were also predicted in the theoretical studies on the co-existence of conductivity and transparency in tin oxide films.[49] The different depth dependence of VB_{onset} and VB_{MAX}, especially the plateau region starting above 1 nm information depth, indicates additional existence of "buried" V_{Sn} in this region, altering the band structure. The overall changes of the stoichiometry and the energy level position should be reproduced correspondingly in the carrier concentration distribution across the SnO_x layer. Negative carrier concentration was determined as[50]

$$n_c = N_c \exp\left(-\frac{E_C - E_F}{kT}\right) \quad (3)$$

where N_c is the effective density of states in the conduction band, for SnO_2 $N_c = 2(\frac{2\pi m_e^* kT}{h^2})^{\frac{3}{2}}$; m_e^* is the states' effective mass of electrons (here, 0.30 in units of the free electron mass m_0, Ref. 51), k is the Boltzmann constant, and T is the absolute temperature, here 300 K. The energetic distance, $E_F - E_c$, is calculated as the difference between the band gap and the value of $E_F - E_V$ obtained from measurements of the VB region. Knowledge of the band gap is crucial here. Literature values range from $E_g = 3.6$ eV (Refs. 52 and 53) for stoichiometric SnO_2 through $E_g = 3.0$ (Ref. 54) for an intermediate form to $E_g = 2.7$ for stoichiometric SnO.[11] Taking into account the calculated stoichiometry (Figure 1), the closest to our layers is $E_g = 2.93$ eV for heavily defective SnO layers, as calculated by Varley *et al.*[46] Basing on the results of Sanon *et al.*, band gap narrowing can be neglected for our results.[55]

Figure 3 shows a compilation of the determined electronic parameters into one band-like diagram. The figure also presents the carrier concentration profile. The change in carrier concentration from nearly insulating at the SnO_x surface, through an intrinsic-like plateau in the middle of the layer to semiconducting at the bottom of the SnO_x film, is significant. The relatively low level of carrier concentration is possibly related to the dominance of SnO, which often behaves as a p-type semiconductor.[11,46] However, it might be expected that the exact value of carrier concentration was influenced by the experiment conditions. The energy level shift of both, core levels and valence levels, is displayed in the main diagram. Black solid lines present the global change in energy levels, while the gray lines show only the electrostatic potential contribution to the energy level change. The difference between global change and electrostatic potential contribution can be assigned to a chemical shift. The direction of energy levels shift in the substrate and the SnO_x layer suggests negative charge displacement[44] from Si substrate over the thin, tunnelable SiO_2 layer[56] into the SnO_x layer. The observed phenomenon is the result of substrate-layer interaction and the change of the layer's composition. The presence of point defects of different nature in the vicinity of the SiO_2/SnO_x interface and SnO_x subsurface area contributes as well. The differences between the valence level shift and the core level shift (~ 0.15 eV) can be

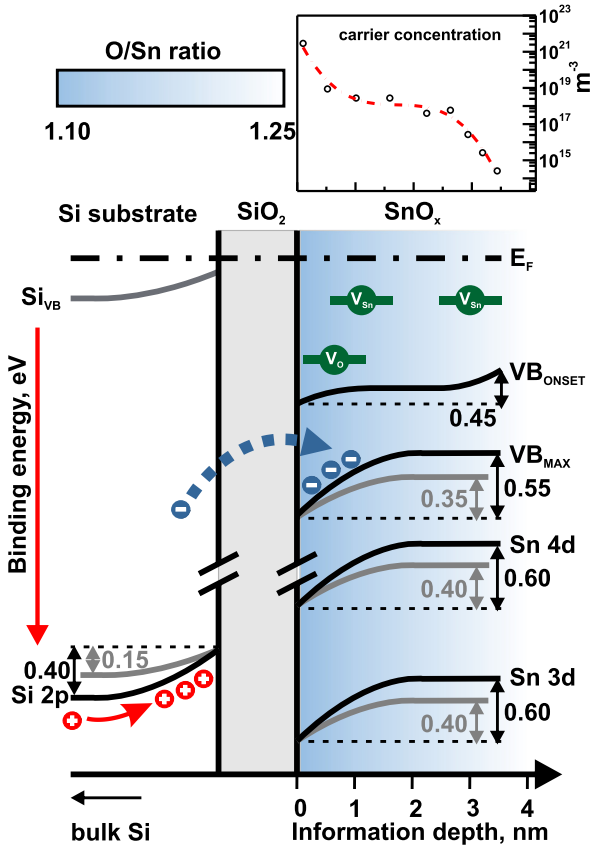

FIG. 3. Band-like diagram for examined $Si/SiO_2/SnO_x$ layer structure. Black solid lines (values) present global change in energy levels, while the gray lines (values) stand for the electrostatic potential contribution to the energy level change. The energy distances below the break are not to scale. Upper panel: Carrier concentration profile, data fitted with a polynomial.

attributed to different defect level impact on the electronic structure: the core levels are most likely shielded from the defect levels placed in the band gap below the Fermi level or just above VB onset. Although the magnitude of the change is relatively small, analysis of the O 1s and Sn3d/4d core level shift shows the origin of detected variation to originate from an alteration of the layer's internal electronic structure, i.e., from chemical shift and inherent electrostatic field across the layer.

Interaction with the environment during the fabrication process also affects the electronic structure of such layers. The drastic decrease in carrier concentration can be attributed to the oxygen uptake from the environment. Surface oxidation strongly decreases the layers' conductivity, reflected by a drop in carrier concentration.[3]

In conclusion, utilizing ADXPS, for sol-gel $SnO_{1<x<2}$ layers of a thickness comparable with the electron attenuation length, the stoichiometry was quantified and electronic structure was determined. Obtained results indicate the downward energy levels shift by 0.45 eV in the SnO_x layers at the SiO_2/SnO_x interface. In combination with detected upward energy levels shift in the substrate, a negative charge displacement via the tunnelable oxide layer must be present. Cumulative result is the carrier concentration gradient from nearly insulating at the SnO_x surface to semiconducting at the bottom of the SnO_x film. Analysis show that the further development of the used cost-effective technology based on

a single-step process may result in films acting as single layer p-n-junction. This is of interest for future low-dimensional electronics and sensor application.

This work was partially supported by the Polish budget for science in years 2013–2015 by Ministry for Science and Higher Education within Iuventus Plus IP2012 019072 project through the Silesian University of Technology, Institute of Physics. Special thanks go to Professor J. Bodzenta, Dr. L. Grządziel, and Dr. A. Bier for continuous support.

[1]M. E. White, O. Bierwagen, M. Y. Tsai, and J. Speck, Appl. Phys. Express **3**, 051101 (2010).
[2]R. B. Wexler and K. Sohlberg, J. Phys. Chem. A **118**, 12031 (2014).
[3]N. Tsuda, *Electronic Conduction in Oxides* (Springer Science & Business Media, 2000).
[4]H. Hosono, Y. Ogo, H. Yanagi, and T. Kamiya, Electrochem. Solid-State Lett. **14**, H13 (2011).
[5]E. Fortunato, R. Barros, P. Barquinha, V. Figueiredo, S.-H. K. Park, C.-S. Hwang, and R. Martins, Appl. Phys. Lett. **97**, 052105 (2010).
[6]H. Yabuta, N. Kaji, R. Hayashi, H. Kumomi, K. Nomura, T. Kamiya, M. Hirano, and H. Hosono, Appl. Phys. Lett. **97**, 072111 (2010).
[7]J.-P. Colinge, C.-W. Lee, A. Afzalian, N. D. Akhavan, R. Yan, I. Ferain, P. Razavi, B. O'Neill, A. Blake, M. White, A.-M. Kelleher, B. McCarthy, and R. Murphy, Nat. Nanotechnol. **5**, 225 (2010).
[8]W. Guo, L. Fu, Y. Zhang, K. Zhang, L. Y. Liang, Z. M. Liu, H. T. Cao, and X. Q. Pan, Appl. Phys. Lett. **96**, 042113 (2010).
[9]P. D. Borges, L. M. R. Scolfaro, H. W. Leite Alves, and E. F. da Silva, Jr., AIP Conf. Proc. **1199**, 124 (2010).
[10]J. E. Dominguez, L. Fu, and X. Q. Pan, Appl. Phys. Lett. **81**, 5168 (2002).
[11]Y. Ogo, H. Hiramatsu, K. Nomura, H. Yanagi, T. Kamiya, M. Hirano, and H. Hosono, Appl. Phys. Lett. **93**, 032113 (2008).
[12]M. Kwoka, L. Ottaviano, P. Koscielniak, and J. Szuber, Nanoscale Res. Lett. **9**, 260 (2014).
[13]G. Sberveglieri, Sens. Actuators, B **23**, 103 (1995).
[14]M. Kwoka and M. Krzywiecki, Mater. Lett. **154**, 1 (2015).
[15]M. Utriainen, H. Lattu, H. Viirola, L. Niinistö, R. Resch, and G. Friedbacher, Mikrochim. Acta **133**, 119 (2000).
[16]M. Krzywiecki, L. Grządziel, A. Sarfraz, D. Iqbal, A. Szwajca, and A. Erbe, Phys. Chem. Chem. Phys. **17**, 10004 (2015).
[17]See www.casaxps.com for curve fitting procedure.
[18]I. Lindau, P. Pianetta, K. Y. Yu, and W. E. Spicer, Phys. Rev. B **13**, 492 (1976).
[19]J. F. Watts and J. Wolstenholme, *Surface Analysis by XPS and AES* (Wiley & Sons, Chichester, 2003).
[20]R. L. Opila and J. Eng, Jr., Prog. Surf. Sci. **69**, 125 (2002).
[21]See http://www.thermoscientific.com/en/product/theta-probe-angle-resolved-x-ray-photoelectron-spectrometer-arxps-system.html for details regarding angle-dependent analysis in photoemission experiments.
[22]P. J. Cumpson, Surf. Interface Anal. **29**, 403 (2000).
[23]W. S. M. Werner, Surf. Interface Anal. **18**, 217 (1992).
[24]S. Tanuma, C. J. Powell, and D. R. Penn, Surf. Interface Anal. **21**, 165 (1994).
[25]C. J. Powell and A. Jablonski, *NIST Electron Inelastic-Mean-Free-Path Database, Version 1.2, SRD 71* (National Institute of Standards and Technology, Gaithersburg, MD, 2010).
[26]J. R. Taylor, *An Introduction to Error Analysis: The Study of Uncertainties in Physical Measurements* (University Science Books, Sausalito, 1997).
[27]D. Ehre and H. Cohen, Appl. Phys. Lett. **103**, 052901 (2013).
[28]A. Rozenblat, Y. Rosenwaks, L. Segev, and H. Cohen, Appl. Phys. Lett. **94**, 053116 (2009).
[29]A. Givon and H. Cohen, Surf. Interface Anal. **47**, 607 (2015).
[30]P. Seah and W. A. Dench, Surf. Interface Anal. **1**, 2 (1979).
[31]See www.lasurface.com/xps/niveau3.php for Sn 3d peak assignment.
[32]T. L. Barr, J. Phys. Chem. **82**, 1801–1810 (1978).
[33]C. D. Wagner, W. M. Riggs, L. E. Davis, J. F. Moulder, and G. E. Milenberger, *Handbook of X-ray Photoelectron Spectroscopy* (Perkin-Elmer, Eden Prairie, MN, 1979).
[34]M. Futsuhara, K. Yoshioka, and O. Takai, Thin Solid Films **322**, 274 (1998).
[35]C. D. Wagner, J. Vac. Sci. Technol. **15**, 518 (1978).
[36]S. Suzer, T. Voscoboinikov, K. R. Hallam, and G. C. Allen, Fresenius J. Anal. Chem. **355**, 654 (1996).
[37]L. C. Lynn and R. L. Opila, Surf. Interface Anal. **15**, 180 (1990).
[38]W. K. Choi, J. S. Cho, J. Cho, S. C. Choi, H.-J. Jung, and S. K. Koh, J. Korean Phys. Soc. **31**, 369 (1997).
[39]S. M. Barlow, P. Bayat-Mokhtari, and T. E. Gallon, J. Phys. C: Solid State Phys. **12**, 5577 (1979).
[40]R. A. Powell, Appl. Surf. Sci. **2**, 397 (1979).
[41]J. Blomquist, J. Electron Spectrosc. Relat. Phenom. **36**, 69 (1985).
[42]J. Blomquist, U. Helgeson, B. Folkesson, R. Larsson, P. Sundberg, and M. Andersson, Hyperfine Interact. **28**, 697 (1986).
[43]H. Cohen, C. Nogues, I. Zon, and I. Lubomirsky, Appl. Phys. Lett. **97**, 113701 (2005).
[44]T. Chasse, C. I. Wu, I. G. Hill, and A. Kahn, J. Appl. Phys. **85**, 6589 (1999).
[45]A. Walsh, D. J. Payne, R. G. Egdell, and G. W. Watson, Chem. Soc. Rev. **40**, 4455 (2011).
[46]J. B. Varley, A. Schleife, A. Janotti, and C. G. Van de Walle, Appl. Phys. Lett. **103**, 082118 (2013).
[47]D. B. Granato, J. A. Caraveo-Frescas, H. N. Alshareef, and U. Schwingenschlogl, Appl. Phys. Lett. **102**, 212105 (2013).
[48]A. Togo, F. Oba, I. Tanaka, and K. Tatsumi, Phys. Rev. B **74**, 195128 (2006).
[49]C. Kilic and A. Zunger, Phys. Rev. Lett. **88**, 095501 (2002).
[50]W. Monch, *Semiconductor Surfaces and Interfaces* (Springer-Verlag, Berlin, 1995).
[51]C. Rodl and A. Schleife, Phys. Status Solidi A **211**, 74 (2014).
[52]N. Chiodini, A. Paleari, D. DiMartino, and G. Spinolo, Appl. Phys. Lett. **81**, 1702 (2002).
[53]V. T. Agekyan, Phys. Status Solidi A **43**(11), 11 (1977).
[54]*Langes Handbook of Chemistry*, 14th ed., edited by J. A. Dean (McGraw-Hill, Inc., New York, 1992).
[55]G. Sanon, R. Rup, and A. Mansingh, Phys. Rev. B **44**, 5672 (1991).
[56]J. Mizsei, Vacuum **67**, 59 (2002).